

Derivation of an Enhanced Pressure Differential Expression, for a Penetration Injection with Back Pressure

Prashant Unnikrishnan Nair

Affiliation1 - Director, Global Categories, Schlumberger Ltd, USA

Affiliation2 - University of North Carolina, Chapel Hill, Kenan Flagler Business School, USA

Corresponding Author: prashantunair@alumni.unc.edu

ABSTRACT

In real-world water injection applications, an in-line injection facilitates a pressure differential that boosts the current flow. A pressure differential created by the injection of a pressurized flow into the mainline of flow is derived from the momentum transfer equation. Heat loss is disregarded, and such empirical equations provide a ballpark value to these pressure differentials during the injection.

In industrial applications, injection of the fluid is done on the surface, due to weld and other constraints where losses due to friction and eddy current formation are imminent. On the other hand, penetration injection provides a far more augmented pressure differential that has a polynomial impact based on the mainline flow rate and the injection flow rate.

This paper aims to derive an accurate representation of the pressure differential values obtained from a penetration injection through experimentation and compare it against a surface injection or empirical calculation. The paper concludes by indicating that the penetration injection augments the pressure differential with a new empirical formula for the derived pressure differential as a polynomial equation for this apparatus and can be extended across different sizes of the mainline and injection line diameters. This work provides a precise formula that can be used to derive pressure differential and estimate the flow and pressure rates. The formula also provides a platform for further utility in the fracturing operations where fracture flow from the well upstream presents multiple injection fractures to the mainline through fracture pores.

Keywords-- Injection Flow, Momentum Transfer, Empirical Equation, Fracturing Pressure, Derivative Calculations

I. INTRODUCTION

Water injection and water flooding are common and vital processes in reservoir development. Low permeability reservoirs that have brittle rocks quickly develop fractures (Laubach, 2003), (Nelson,1985) while such water pumping serves to improve the oil recovery (Morrow and Buckley, 2011). Injected water can cause intense flooding through the cracks of the soil and thereby

result in a reduced effectivity (Shedid, 2006),(Wang et al.,2011). Therefore, it is important to accurately know water injection pressure of such permeable reservoirs (Lyu et al., 2018).

Any flow of water can be boosted by utilizing an injection line across the main pipeline. The pressure differential across the mainline is therefore increased using the added injection. For this paper's purpose, we focus on the derivation of the pressure differential across the mainline by the phenomenon of mass transfer using a flushed and penetrated injection methodology and comparing it to the empirical momentum transfer equation. This paper does not detail the fracturing phenomenon based on well pattern development or on rock acoustics emission experiments (Amadei, 2012), (Brudy et al., 1997), (Michihiro et al., 1985) instead, only the pressure differential phenomenon through different injection model is of interest.

Theoretically, the differential pressure across any mainline can be increased by providing a boost line (called injector) to the main flow. The deferential pressure increment can be directly obtained from the principle of momentum transfer (Corcoran,1956) applied in a controlled volume and is given by the formula (1):

$$\Delta P = \frac{\rho}{A_{Pipe}} + \left(\frac{Q_{Inject}^2}{A_{Inject}} * \cos \alpha + \frac{Q_{Pipe}^2}{A_{Pipe}} - \frac{(Q_{Inject} + Q_{Pipe})^2}{A_{Pipe}} \right) \quad (1)$$

Qjet = flow rate through the jet pipe
 Qpipe = inlet flow rate through the main pipe
 Ajet = jet pipe cross-section area
 Apipe = main pipe cross-section area
 ρ = water density
 α = angle between jet pipe and main pipe
 ΔP = Pressure differential across a section of flow.

Losses as heat generated are ignored in this equation. The differential pressure allows for a boost in the main line with increased pressure. When used as it is with the inlet stream immersed into the main line flow, the concept is valid only when used as it is. The dependency on a streamed surface or flushed surface push in contrast with an immersed inclusion provides different results with

respect to the boost pressure affecting the speed of flow across the sections.

An experimental determination is discussed to verify this and generate a new empirical calculation for the enhanced pressure differential for a setup with restricted flow and developed backpressure.

The formulae derived is limited to the experimental setup but provides a base for expansion to other research work that have similar scenarios.

II. MATERIAL AND METHODS

2.1 Setup

As detailed in Figure 1, the setup consists of a custom-made test fixture connected to a water tank. Two centrifugal pumps attached to the tank allow water to be pulled from the source and circulate through the test fixture. Water pumped by mainline flow CP1 enters the fixture through the bulkhead ports B1 and B3, while water pumped by flow injector pump enters through the inlet ports I1 and I2 (depending on the test scenario). Fluid flows through the pipe and then returns to the tank through outlet ports O1 and O3. Ports B2 and O2 were provided in the event an extra flow is required (not intended to be used otherwise).

Flowmeters for the mainline and the injector line were positioned, respectively, all along the setup to allow the water flow rate to be measured throughout the test. An ARDIC converter was used to measure and store all variables to run quick simulations and obtain graph results (Lu et al.,2019), (Nagarsheth & Nair, 2021).

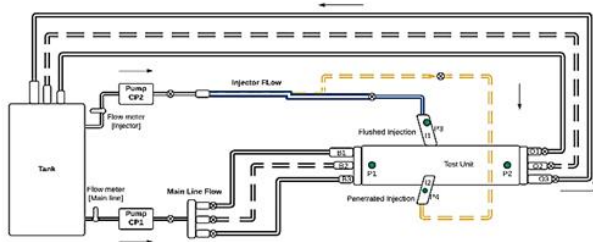


Figure 1: Schematic layout of the experimental setup

P1 and P2 are Pressure gauges to measure pressure across the test unit. At the same time, P3 and P4 are pressure gauges to measure the pressure at the flushed injector and penetrated injector based on their usage, respectively. All flow lines were provided with necessary ball valves to enable opening and closing of flow as required for the experiment.

The test fixture designed as an “at-scale” representation of the true process piping boost pipe for an application is further detailed in Figure 2.

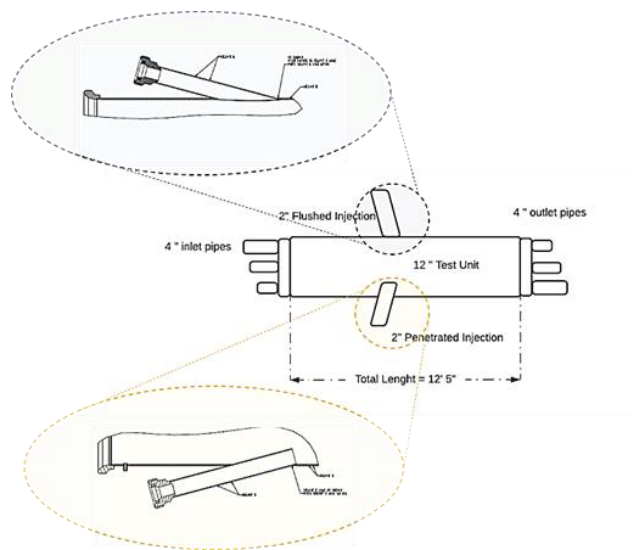


Figure 2: Detail of the test fixture made to scale for the application

The test fixture includes two injector geometries: flushed injector and penetrating injector. For research, the experiments were carried out and identically performed through each of these geometries independently to ascertain the difference across the injector pressure and overall performance, to compare each geometry effectiveness. Figure 3 details the test layout as physically implemented on the shop floor.



Figure 3: Overview of test setup and details of test fixture. Injector pipe (left) and full piping system (right)

2.2 Test Plan Requirements

Fundamentally, it was identified that four criteria are required to be determined. These are

- the pressure drop created across the injector pipe, for various values of the flow through the boost pipe
- sensitivity of the differential pressure to the flow made through the main pipe,
- effect of different injection rate
- influence of the injector pipe geometry on the differential pressure.

For a flushed injector geometry, the injector pipe flow rate was set to 10 barrels per minute (BPM). The following steps were then carried out.

- Vary the flow rate through the main pipe, from 0 BPM to 35 BPM (5 BPM increment); measured at the flowmeter main line
- Measure the pressure at the inlet of the main pipe, at the outlet, and the differential pressure across the boost pipe.

Once the results were collected, the process was repeated with changes in boost flow rate at 15 BPM and 20 BPM; measured at flow meter injector, and data captured. Similarly, the experiment was repeated for the penetration injector geometry 2 and data recorded separately (Fraser et al., 2007), (Van den Eynde et al., 2019).

III. OBSERVATION AND DISCUSSION

3.1 Boost Pressure Comparison for Various Main Pipe Flow Rates

Pressure differentials across the main pipe is check for various flow rates at the mainline and injector line. As there are two different geometries, data is collected across each and compared to the empirical equation that does not define the injection geometry.

Empirical Injection

The theoretical pressure drop across the boost pipe as a function of the main pipe flow rate is represented in Figure 4.

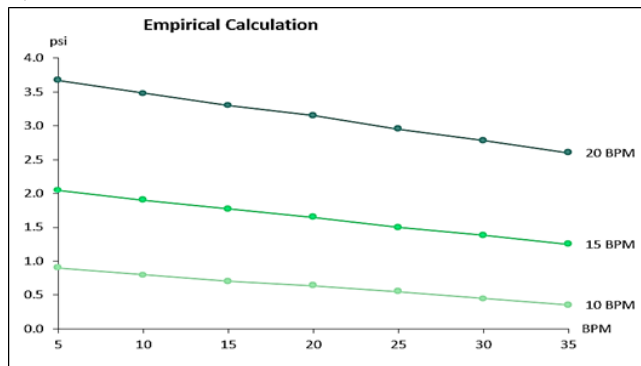


Figure 4: Empirically calculated differential pressure for various flow rates.

It can be observed that

- for a given flow in the main pipe, pressure drop increases when boost flow increases
- for a given flow in the boost pipe, pressure drop decreases when the main flow increases.

Flushed/Surface Injection

For a flushed injection geometry in Figure 2, data on the differential pressure across boost and the main flow is demonstrated in Figure 5.

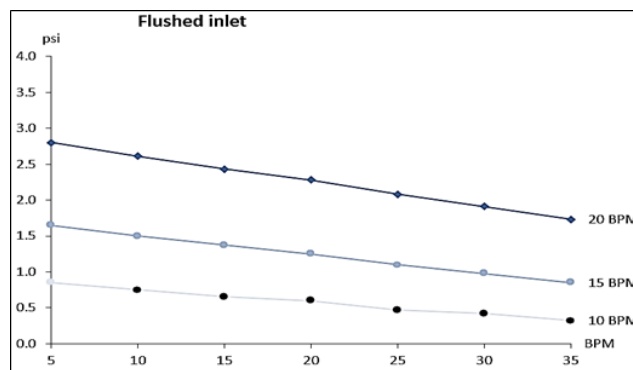


Figure 5: Differential pressure for various flow rates on flushed injector geometry

Based on the data gathered and plotted in Figure 5 that the empirical values from Figure 4 do not account for the various losses in heat etc., during the flow of the fluid. This accounts for why the pattern of the graphs in both cases are similar, however the flushed inlet model has a lowered differential pressure than that of obtained from an empirical calculation.

Penetrated Injection

For a penetrated geometry, data gathered on the differential pressure across boost and main flow in Figure 2 is represented in Figure 6.

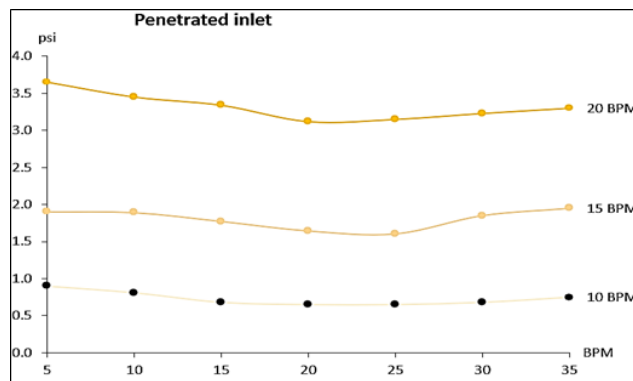


Figure 6: Differential pressure for various flow rates on penetrated injector geometry

3.2 Injector Pressure Comparison across the Different Geometry of Penetration for Varying Main Line Flow and Fixed Injector Flow

For the second part of the study, data for all observations made is compared to each other at specific injection rates to see the pressure differential behavior across the pipeline for a given flow and a fixed injection flow rate as the rate is increased. This further allows comparing the effect of injector geometry with that of each other alongside the empirical calculation at those fixed flow rates on

Recordings are taken for each result obtained are represented in Figure 7 through Figure 9.

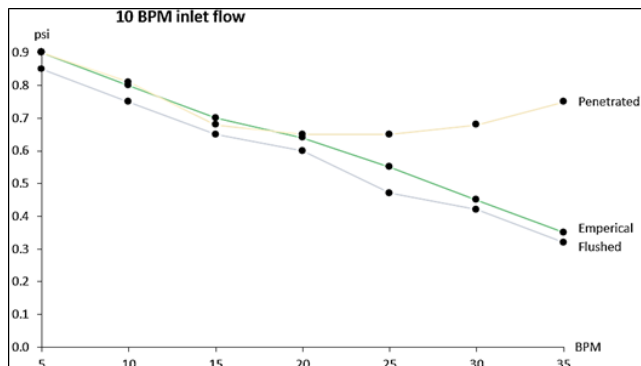


Figure 7: Differential pressure for a 10 BPM flow rate at injector

At 10 BPM, the flushed injection trend is similar to the empirical trend, but with pressure drop losses. Penetrated injection almost always follows the empirical equation trend until the line pressure is greater than 20 BPM and then deviates sharply upward to provide a better differential pressure.

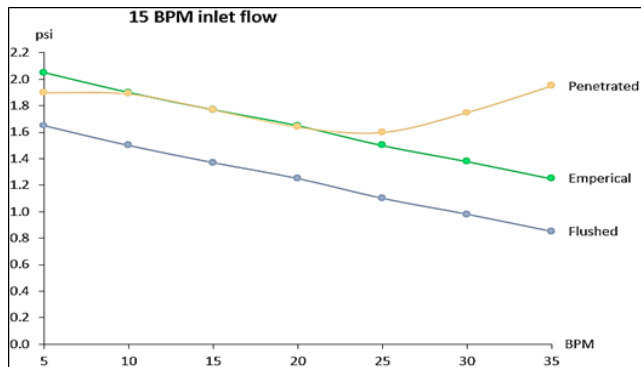


Figure 8: Differential pressure for a 15 BPM flow rate at injector

Like 10 BPM, a study at 20 BPM also reveals that the flushed injection trend is similar to the empirical trend, but with pressure drop losses. Penetrated injection always follows the empirical equation trend until a line pressure of 20 BPM and then deviates sharply upward.

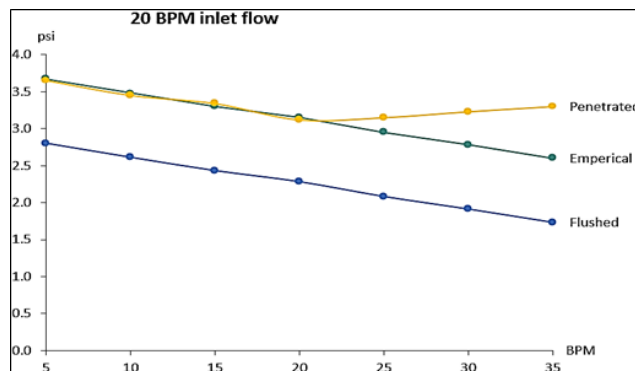


Figure 9: Differential pressure for a 20 BPM flow rate at injector

Like 10 BPM and 20 BPM, the penetration injection provides a better pressure differential and deviates from the empirical values when the line pressure is higher than 20 BPM.

Deviation and the gap in pressure differential between the two geometries, the impact across the boost line and the mainline is captured. Figure 10 depicts the behavior of penetrated and flushed injection for various flow rates of the mainline. The figure allows us to see the behavior and understand the gap across the multiple flow rates and pressure differentials created across the two geometries.

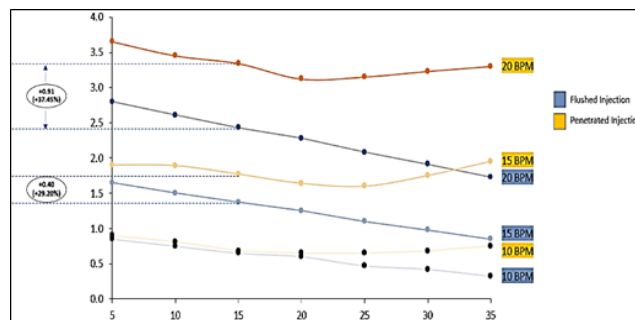


Figure 10: Differential pressure for various flow rates across flushed and penetrated geometry

A similar comparison of the penetration injection against the empirical values is represented in Figure 11. it can be observed that penetration geometry follows the same trend as the empirical calculations until the mainline exceeds a 20 BPM flow rate. Post 20 BPM flow rate at the mainline, the pressure differential provided by penetration injection exceeds that of the empirical calculation. The pressure differential for the flow after 20 BPM at the mainline gaps according to the injector flow rate.

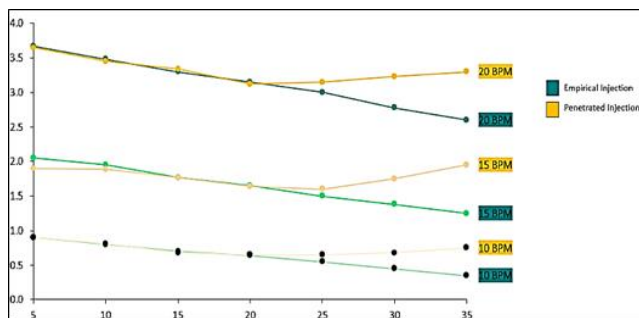


Figure 11: Differential pressure for various flow rates between a penetration injection and empirical values represented as a side-by-side value for comparison

Figure 12 demonstrates the gaps between the empirical calculations and the data obtained for a flushed injection. It is clear from the figure that the flushed injection geometry follows the same trends as that of the empirical calculations but with a dipped value in pressure differential. The gap between the two depends on the injector flow rate levels.

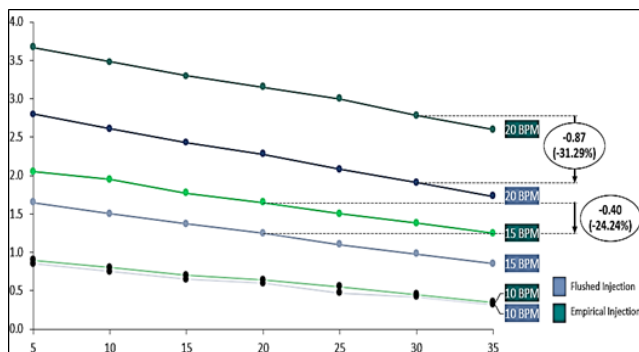


Figure 12: Differential pressure for various flow rates between a flushed injection and empirical values

IV. RESULTS AND CONCLUSION

It is first observed that whatever the flow rate is, the penetrating injector geometry creates a higher pressure drop than the flushed pipe. This is a decisive conclusion as the penetrating injection generates a boost, which converges toward the main flow stream flowing the science of momentum transfer. In contrast, the flushed pipe generates a more divergent flow boost with eddy formations. The flushed injection is shown in Figure 12 clearly demonstrates that the empirical calculation does not consider the loss of momentum as heat from eddy currents formed by the injection of fluid. As there is a higher momentum loss with a higher injection rate, the average gap of 0.87 and 0.40 in pressure differential is understandable. This drop in pressure differential also

accounts for frictional and other losses that play in a flow, thereby causing a reduction.

Further, the penetrated injection follows the empirical calculation until 20 BPM at the mainline regardless of the injection flow rate. Beyond the 20 BPM flow rate at the mainline, an increase in the mainline flow rate spikes a pressure differential increase. At the 10 BPM injection flow rate, the increase in pressure is 0.15, 0.45, and 0.75, respectively, at 25, 30, and 35 BMP of the mainline flow. Similar pressure differential increases beyond the 20 BMP mainline flow rate are visible at injection flow rates of 15 and 20 BPM. This increase will be beyond the 35 to 40 BMP at some point plateau as the system's backpressure increases with the mainline flow rate.

Further, we can conclude that the penetration injection augments the fluid flow to a certain extent, enhances the pressure differential value, and is not captured in the mass transfer equation for our setup.

From Figure 6, we have already established that the pressure variance is not a linear function like the empirical equation based on momentum transfer. As the data collected for pressure differential in a penetrated line is through experimentation in real-time, pressure spikes at the gauges are expected. We know the turbulence is higher at higher injection. For calculation and derivation purposes, we will consider the data at 10 BPM at injection, where the pressure gauges are least strained to derive the closest accurate value of the differential pressure (De Cock et al.,2012), (Li and Horne,2003), (Ostertagova,2012). A magnified image of the same with a distinctive equation at 10 BPM based on Figure 6 is represented in figure 13.

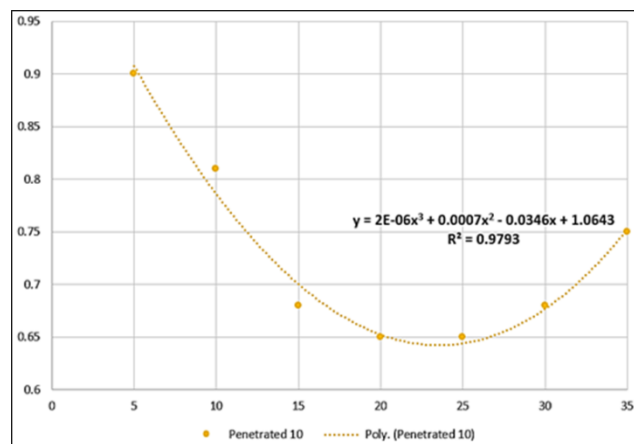


Figure 13: Differential pressure for penetration injection against empirical values

Similarly, the pressure differential of the penetrated injection and that derived from the empirical equation for the same flow rate in the mainline and for an injection flow rate can be plotted against the pressure

differentials data on the empirical values, as shown in figure 15.

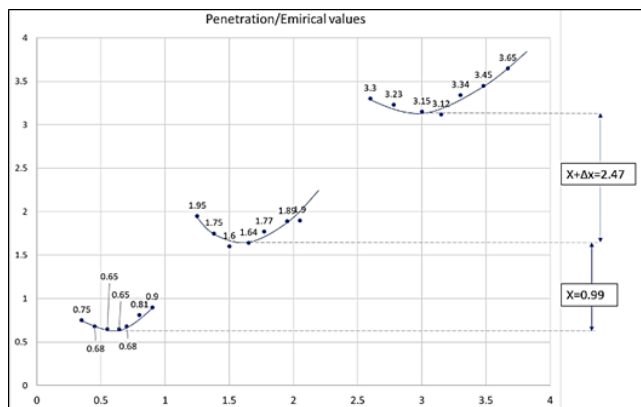


Figure 14: Differential pressure for penetration injection for each empirical value as the base

A magnified version of the data in figure 14 at 10 BPM injection rate with change in Y and X-axis range is then explored again for the region of least spikes when data gathering and can plotted as shown in figure 16.

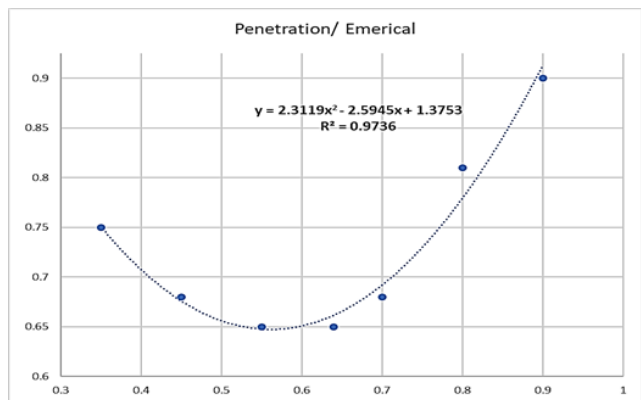


Figure 15: Differential pressure for penetration injection at 10 BPM main line flow

From the derivative at 10 BPM, the pressure differential for a penetrated injection can be re-written as

$$\Delta P_{10} = 2.3119 * \left(\frac{\rho}{A_{Pipe}} + \left(\frac{Q_{Inject}^2}{A_{Inject}} * \cos \alpha + \frac{Q_{Pipe}^2}{A_{Pipe}} - \frac{(Q_{Inject} + Q_{Pipe})^2}{A_{Pipe}} \right)^2 \right) - 2.5945 \left(\frac{\rho}{A_{Pipe}} + \left(\frac{Q_{Inject}^2}{A_{Inject}} * \cos \alpha + \frac{Q_{Pipe}^2}{A_{Pipe}} - \frac{(Q_{Inject} + Q_{Pipe})^2}{A_{Pipe}} \right)^2 \right) + 1.3753 \tag{2}$$

$$\Delta P_{15} = 2.3119 * \left(\frac{\rho}{A_{Pipe}} + \left(\frac{Q_{Inject}^2}{A_{Inject}} * \cos \alpha + \frac{Q_{Pipe}^2}{A_{Pipe}} - \frac{(Q_{Inject} + Q_{Pipe})^2}{A_{Pipe}} \right)^2 \right) - 2.5945 \left(\frac{\rho}{A_{Pipe}} + \left(\frac{Q_{Inject}^2}{A_{Inject}} * \cos \alpha + \frac{Q_{Pipe}^2}{A_{Pipe}} - \frac{(Q_{Inject} + Q_{Pipe})^2}{A_{Pipe}} \right)^2 \right) + 2.32753 \tag{3}$$

$$\Delta P_{20} = 2.3119 * \left(\frac{\rho}{A_{Pipe}} + \left(\frac{Q_{Inject}^2}{A_{Inject}} * \cos \alpha + \frac{Q_{Pipe}^2}{A_{Pipe}} - \frac{(Q_{Inject} + Q_{Pipe})^2}{A_{Pipe}} \right)^2 \right) - 2.5945 \left(\frac{\rho}{A_{Pipe}} + \left(\frac{Q_{Inject}^2}{A_{Inject}} * \cos \alpha + \frac{Q_{Pipe}^2}{A_{Pipe}} - \frac{(Q_{Inject} + Q_{Pipe})^2}{A_{Pipe}} \right)^2 \right) + 3.80753 \tag{4}$$

For each of the above cases, the injector influence is negated and built inside the fixed constant value that changes as the injector flow changes. That is, for injector flow at 10 BPM, the constant is 1.3753, for 20 BPM is 2.32753, and for 30 BPM it is 3.80753. Based on (Dutka and Ewens,1971), the pressure differential equation therefore, can be rewritten as

$$P_{new} = 2.3119 * \left(\frac{\rho}{A_{Pipe}} + \left(\frac{Q_{Inject}^2}{A_{Inject}} * \cos \alpha + \frac{Q_{Pipe}^2}{A_{Pipe}} - \frac{(Q_{Inject} + Q_{Pipe})^2}{A_{Pipe}} \right)^2 \right) - 2.5945 \left(\frac{\rho}{A_{Pipe}} + \left(\frac{Q_{Inject}^2}{A_{Inject}} * \cos \alpha + \frac{Q_{Pipe}^2}{A_{Pipe}} - \frac{(Q_{Inject} + Q_{Pipe})^2}{A_{Pipe}} \right)^2 \right) + f(Q_{Inject}) \tag{5}$$

As the fixed variants 1.3753, 2.3753, and 3.80753 are values that depend on the injection flow rate putting the values of the intercepts in the equation against the injector flow rate, we can observe that f(QInject) can be presented by the equation as shown in Figure 16.

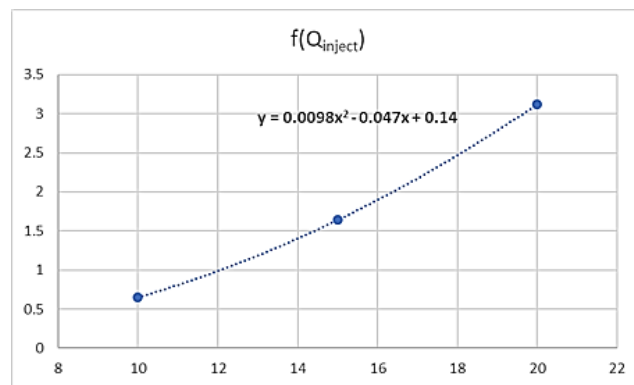


Figure 16: Differential pressure for penetration injection at various injection flow rates

We can therefore conclude the final equation as

$$\Delta P_{new} = 2.3119 * \left(\frac{\rho}{A_{Pipe}} + \left(\frac{Q_{Inject}^2}{A_{Inject}} * \cos \alpha + \frac{Q_{Pipe}^2}{A_{Pipe}} - \frac{(Q_{Inject} + Q_{Pipe})^2}{A_{Pipe}} \right)^2 \right) - 2.5945 \left(\frac{\rho}{A_{Pipe}} + \left(\frac{Q_{Inject}^2}{A_{Inject}} * \cos \alpha + \frac{Q_{Pipe}^2}{A_{Pipe}} - \frac{(Q_{Inject} + Q_{Pipe})^2}{A_{Pipe}} \right)^2 \right) + 0.0098Q_{Inject}^2 - 0.047Q_{Inject} + 0.14 \tag{6}$$

V. CLOSING STATEMENT OR CONCLUSION

Equation (6) provides a better pressure differential value for all purposes compared with the momentum transfer equation for our application, restricted to the experimental setup and the backpressure produced due to the experimental constraints and restricted flow.

For the next part, researchers can explore the empirical equations variations based on the depth of the penetration at the injector using fluid dynamics and the transfer of momentum calculations. Researchers in confined volume injection and processes such as fracturing can further study injection behavior based on the

restrictions of the process. For example, every fracturing space similar to the experimental setup of the article has variables in burial depth, pore fluid pressure, present-day stress, and mainline flow that can be used in the derived equation to enhance fracturing dynamics.

REFERENCES

- [1] Amadei, B. & Stephansson, O. (2012). *Rock stress and its measurement*. (1997th ed.). Springer.
- [2] Brudy, M., Zoback, M. D., Fuchs, K., Rummel, F., & Baumgärtner, J. (1997). Estimation of the complete stress tensor to 8 km depth in the KTB scientific drill holes: Implications for crustal strength. *Journal of Geophysical Research: Solid Earth*, 102(B8), 18453–18475. Available at: <https://doi.org/10.1029/96jb02942>.
- [3] Corcoran, W. H. (2012). *Momentum transfer in fluids*. Academic Press.
- [4] De Cock, M. (2012). Representation use and strategy choice in physics problem solving. *Physical Review Special Topics - Physics Education Research*. Available at: <https://doi.org/10.1103/physrevstper.8.020117>.
- [5] Dutka, A. F. & Ewens, F. J. (1971). A method for improving the accuracy of polynomial regression analysis. *Journal of Quality Technology*, 3(4), 149–155. Available at: <https://doi.org/10.1080/00224065.1971.11980487>.
- [6] Nelson R. A. (1986). *Geologic analysis of naturally fractured reservoirs*. Contributions in Petroleum Geology & Engineering Series no. 1. xvi + 320pp. Houston, London, Paris, Tokyo: Gulf. Price £42.00 (hardback). ISBN 0 87201 575 0. U.K. and European distributors: Kogan Page Ltd, 120 Pentonville Road, London N1 9JN. *Geological Magazine*, 124(4), 387–388. Available at: <https://doi.org/10.1017/s0016756800016794>.
- [7] Fraser, D. M., Pillay, R., Tjatindi, L., & Case, J. M. (2007). Enhancing the learning of fluid mechanics using computer simulations. *Journal of Engineering Education*, 96(4), 381–388. Available at: <https://doi.org/10.1002/j.2168-9830.2007.tb00946.x>.
- [8] Laubach, S. E. (2003). Practical approaches to identifying sealed and open fractures. *AAPG Bulletin*, 87(4), 561–579. Available at: <https://doi.org/10.1306/11060201106>.
- [9] Li, K. & Horne, R. N. (2003). A decline curve analysis model based on fluid flow mechanisms. *SPE Western Regional/AAPG Pacific Section Joint Meeting*. Available at: <https://doi.org/10.2118/83470-ms>.
- [10] Lianbo, Z. & Xiang-Yang, L. (2009). Fractures in sandstone reservoirs with ultra-low permeability: A case study of the Upper Triassic Yanchang Formation in the Ordos Basin, China. *AAPG Bulletin*, 93(4), 461–477. Available at: <https://doi.org/10.1306/09240808047>.
- [11] Lu, J., Zhu, X., Peters, E. A. J. F., Verzicco, R., Lohse, D., & Kuipers, J. A. M. (2019). Moving from momentum transfer to heat transfer – A comparative study of an advanced Graetz-Nusselt problem using immersed boundary methods. *Chemical Engineering Science*, 198, 317–333.
- [12] Lyu, W., Zeng, L., Chen, M., Qiao, D., Fan, J., & Xia, D. (2018). An approach for determining the water injection pressure of low-permeability reservoirs. *Energy Exploration & Exploitation*, 36(5), 1210–1228. Available at: <https://doi.org/10.1177/0144598718754374>.
- [13] Michihiro, K., Fujiwara, T., & Yoshioka, H. (1986). Research and engineering applications in rock masses. Proceedings of the 26th US symposium on rock mechanics, rapid city, 26–28 June 1985. 2 vols. *International Journal of Rock Mechanics and Mining Sciences & Geomechanics Abstracts*, 23(4), 125. Available at: [https://doi.org/10.1016/0148-9062\(86\)90647-9](https://doi.org/10.1016/0148-9062(86)90647-9).
- [14] Morrow, N. & Buckley, J. (2011). Improved oil recovery by low-salinity water flooding. *Journal of Petroleum Technology*, 63(05), 106–112. Available at: <https://doi.org/10.2118/129421-jpt>.
- [15] Nagarsheth, H. J., & Nair, P. U. (2002, Aug). Robot interfacing with ARDIC. *Proceedings of the Second International Conference on Manufacturing – ICM*, 3(2), 285-294. Available at: https://figshare.com/articles/conference_contribution/Advance_Robot_Direct_Interface_Controller/13669067/2.
- [16] Ostertagová, E. (2012). Modelling using Polynomial Regression. *Procedia Engineering*, 48, 500–506. Available at: <https://doi.org/10.1016/j.proeng.2012.09.545>.
- [17] Shedid, S. A. (2006). Influences of fracture orientation on oil recovery by water and polymer flooding processes: An experimental approach. *Journal of Petroleum Science and Engineering*, 50(3–4), 285–292. Available at: <https://doi.org/10.1016/j.petrol.2005.12.002>.
- [18] Van den Eynde, S., van Kampen, P., Van Dooren, W., & De Cock, M. (2019). Translating between graphs and equations: The influence of context, direction of translation, and function type. *Physical Review Physics Education Research*, 15(2). Available at: <https://doi.org/10.1103/physrevphyseduces.15.020113>.